

# <sup>18</sup>F-AV-1451 positron emission tomography in Alzheimer's disease and progressive supranuclear palsy

Luca Passamonti,<sup>1,2,\*</sup> Patricia Vázquez Rodríguez,<sup>1,\*</sup> Young T. Hong,<sup>1,3</sup> Kieren S. J. Allinson,<sup>4</sup> David Williamson,<sup>3</sup> Robin J. Borchert,<sup>1</sup> Saber Sami,<sup>1</sup> Thomas E. Cope,<sup>1</sup> W. Richard Bevan-Jones,<sup>5</sup> P. Simon Jones,<sup>1</sup> Robert Arnold,<sup>5</sup> Ajenthan Surendranathan,<sup>5</sup> Elijah Mak,<sup>5</sup> Li Su,<sup>5</sup> Tim D. Fryer,<sup>1,3</sup> Franklin I. Aigbirhio,<sup>1,3</sup> John T. O'Brien<sup>5,#</sup> and James B. Rowe<sup>1,6,#</sup>

\*,#These authors contributed equally to this work.

The ability to assess the distribution and extent of tau pathology in Alzheimer's disease and progressive supranuclear palsy *in vivo* would help to develop biomarkers for these tauopathies and clinical trials of disease-modifying therapies. New radioligands for positron emission tomography have generated considerable interest, and controversy, in their potential as tau biomarkers. We assessed the radiotracer <sup>18</sup>F-AV-1451 with positron emission tomography imaging to compare the distribution and intensity of tau pathology in 15 patients with Alzheimer's pathology (including amyloid-positive mild cognitive impairment), 19 patients with progressive supranuclear palsy, and 13 age- and sex-matched controls. Regional analysis of variance and a support vector machine were used to compare and discriminate the clinical groups, respectively. We also examined the <sup>18</sup>F-AV-1451 autoradiographic binding in post-mortem tissue from patients with Alzheimer's disease, progressive supranuclear palsy, and a control case to assess the <sup>18</sup>F-AV-1451 binding specificity to Alzheimer's and non-Alzheimer's tau pathology. There was increased <sup>18</sup>F-AV-1451 binding in multiple regions in living patients with Alzheimer's disease and progressive supranuclear palsy relative to controls [main effect of group,  $F(2,41) = 17.5$ ,  $P < 0.0001$ ; region of interest  $\times$  group interaction,  $F(2,68) = 7.5$ ,  $P < 0.00001$ ]. More specifically, <sup>18</sup>F-AV-1451 binding was significantly increased in patients with Alzheimer's disease, relative to patients with progressive supranuclear palsy and with control subjects, in the hippocampus and in occipital, parietal, temporal, and frontal cortices ( $t$ 's  $> 2.2$ ,  $P$ 's  $< 0.04$ ). Conversely, in patients with progressive supranuclear palsy, relative to patients with Alzheimer's disease, <sup>18</sup>F-AV-1451 binding was elevated in the midbrain ( $t = 2.1$ ,  $P < 0.04$ ); while patients with progressive supranuclear palsy showed, relative to controls, increased <sup>18</sup>F-AV-1451 uptake in the putamen, pallidum, thalamus, midbrain, and in the dentate nucleus of the cerebellum ( $t$ 's  $> 2.7$ ,  $P$ 's  $< 0.02$ ). The support vector machine assigned patients' diagnoses with 94% accuracy. The post-mortem autoradiographic data showed that <sup>18</sup>F-AV-1451 strongly bound to Alzheimer-related tau pathology, but less specifically in progressive supranuclear palsy. <sup>18</sup>F-AV-1451 binding to the basal ganglia was strong in all groups *in vivo*. Postmortem histochemical staining showed absence of neuromelanin-containing cells in the basal ganglia, indicating that off-target binding to neuromelanin is an insufficient explanation of <sup>18</sup>F-AV-1451 positron emission tomography data *in vivo*, at least in the basal ganglia. Overall, we confirm the potential of <sup>18</sup>F-AV-1451 as a heuristic biomarker, but caution is indicated in the neuropathological interpretation of its binding. Off-target binding may contribute to disease profiles of <sup>18</sup>F-AV-1451 positron emission tomography, especially in primary tauopathies such as progressive supranuclear palsy. We suggest that <sup>18</sup>F-AV-1451 positron emission tomography is a useful biomarker to assess tau pathology in Alzheimer's disease and to distinguish it from other tauopathies with distinct clinical and pathological characteristics such as progressive supranuclear palsy.

Received August 28, 2016. Revised November 2, 2016. Accepted November 24, 2016. Advance Access publication January 24, 2017

© The Author (2017). Published by Oxford University Press on behalf of the Guarantors of Brain.

This is an Open Access article distributed under the terms of the Creative Commons Attribution License (<http://creativecommons.org/licenses/by/4.0/>), which permits unrestricted reuse, distribution, and reproduction in any medium, provided the original work is properly cited.

- 1 Department of Clinical Neurosciences, University of Cambridge, Cambridge, UK
- 2 Istituto di Bioimmagini e Fisiologia Molecolare, Consiglio Nazionale delle Ricerche, Milano, Italy
- 3 Wolfson Brain Imaging Centre, University of Cambridge, Cambridge, UK
- 4 Department of Histopathology, Cambridge University Hospital, Cambridge, UK
- 5 Department of Psychiatry, University of Cambridge, Cambridge, UK
- 6 Medical Research Council, Cognition and Brain Sciences Unit, Cambridge, UK

Correspondence to: Dr Luca Passamonti,  
Department of Clinical Neurosciences, University of Cambridge,  
CB2 0SZ, UK  
E-mail: lp337@medschl.cam.ac.uk

**Keywords:** PET; neurodegeneration; tau; Alzheimer's disease; progressive supranuclear palsy

**Abbreviations:** BP<sub>ND</sub> = non-displaceable binding potential; MCI = mild cognitive impairment; PiB = Pittsburgh compound B; PSP = progressive supranuclear palsy

## Introduction

Alzheimer's disease and progressive supranuclear palsy (PSP) are both associated with abnormal accumulation of misfolded and aggregated tau protein. In Alzheimer's disease, oligomeric and aggregated neurofibrillary tau tangles are a major determinant of synaptic/cell dysfunction and death (Goedert *et al.*, 1988; Ballatore *et al.*, 2007; de Calignon *et al.*, 2012), notwithstanding the importance of amyloid- $\beta$  in its 'toxic alliance' with pathological tau (Bloom, 2014). The intensity and distribution of tau in Alzheimer's disease also correlates with the clinical syndrome and severity and has been considered as one of the primary factors in the neuropathological staging of Alzheimer's disease (Braak *et al.*, 2006; Murray *et al.*, 2014; Ossenkoppele *et al.*, 2015).

In patients with PSP and in analogous murine models, intra-neuronal and astrocytic aggregates of pathological tau isoforms (in the form of straight filaments) characterize and promote neurodegeneration (Clavaguera *et al.*, 2013). Furthermore, tau pathology is common in other neurological diseases such as fronto-temporal dementia (Hodges *et al.*, 2004), corticobasal degeneration, and may modulate the course of Parkinson's disease (Spillantini and Goedert, 2001; Irwin *et al.*, 2013), Huntington's disease (Fernández-Nogales *et al.*, 2014), and multiple sclerosis (Anderson *et al.*, 2008).

Despite the importance of tau pathology in several neurological diseases, it has only recently become possible to assess it using brain imaging in living humans. To be able to measure the burden and distribution of tau pathology in living patients, or those at high risk of developing tau-related disorders, would be a major step forward in the development of disease-modifying therapies targeting the tau protein. Specific markers could also enable pathological characterization of syndromes associated with multiple alternate pathologies, such as frontotemporal dementia and corticobasal degeneration (Alexander *et al.*, 2014). Such biomarkers would ultimately need to be assessed in longitudinal studies and clinical trials, but cross-sectional studies

can assess critical properties such as sensitivity to the presence of different diseases and the expected distribution of pathology.

Radioligands have recently been developed for PET to measure *in vivo* binding to aggregated tau, including PBB3 (Maruyama *et al.*, 2013), THK compounds (Okamura *et al.*, 2014), and <sup>18</sup>F-AV-1451 (Chien *et al.*, 2013; Xia *et al.*, 2013). In autoradiographic studies with post-mortem human brain tissues, the radiotracer <sup>18</sup>F-AV-1451 co-localizes selectively with hyperphosphorylated tau over amyloid- $\beta$  plaques (Marquié *et al.*, 2015). In patients with mild cognitive impairment (MCI) and Alzheimer's disease, there is higher <sup>18</sup>F-AV-1451 binding in frontal, parietal, and temporal cortices relative to age-matched healthy controls (Okello *et al.*, 2009). Progressively increasing regional <sup>18</sup>F-AV-1451 binding in Alzheimer's disease has also been associated with Braak staging of neurofibrillary tau pathology (Schöll *et al.*, 2016; Schwarz *et al.*, 2016), while <sup>18</sup>F-AV-1451 PET binding patterns mirror the clinical and neuro-anatomical variability in the Alzheimer's disease spectrum (Ossenkoppele *et al.*, 2016). Specifically, patients with the amnesic presentation of Alzheimer's disease showed the highest <sup>18</sup>F-AV-1451 uptake in medial temporal lobe regions including the hippocampus, while patients with the logopenic variant of Alzheimer's disease displayed increased left hemispheric <sup>18</sup>F-AV-1451 binding, particularly in posterior temporo-parietal areas implicated in linguistic processes (Ossenkoppele *et al.*, 2016). Performance on domain-specific neuro-psychological tests was also associated with increased <sup>18</sup>F-AV-1451 uptake in brain regions involved in episodic memory, visuo-spatial skills, and language production or comprehension (Ossenkoppele *et al.*, 2016).

Nevertheless, critical issues remain unresolved, and in particular the value of <sup>18</sup>F-AV-1451 in differentiating distinct tauopathies as well as the specificity of binding to tau as verified through pathological analyses. Neuropathological data with autoradiography have suggested that the <sup>18</sup>F-AV-1451 tracer displays strong binding to paired helical filaments characteristic of Alzheimer's disease (e.g. intra-neuronal and extra-neuronal neurofibrillary

tangles and dystrophic neurites), but it does not bind so specifically to the straight tau filaments that are more typical of PSP and non-Alzheimer's disease tauopathies (e.g. cortico-basal degeneration) (Marquie *et al.*, 2015). However, we have recently found that  $^{18}\text{F}$ -AV-1451 binds to regions of pathology (i.e. frontal and temporal cortices) in a patient with a *MAPT* gene mutation leading to straight tau filaments and non-Alzheimer's disease dementia (Bevan-Jones, 2016b). It has also been proposed that the  $^{18}\text{F}$ -AV-1451 tracer displays off-target binding, specifically to neuromelanin-containing cells. This was supported by evidence in patients with Parkinson's disease, *in vivo*, in the midbrain; and post-mortem, in retinal and brain tissues in porcine and rodent models (Hansen *et al.*, 2016).

In this study, we sought to evaluate the utility of  $^{18}\text{F}$ -AV-1451 PET imaging in Alzheimer's disease versus non-Alzheimer's disease tauopathies. We used dynamic PET imaging with kinetic modelling, rather than standardized uptake value ratios (SUVR), in part to accommodate variations in cerebral perfusion that can reduce reliability of SUVR. We aimed to identify the patterns of  $^{18}\text{F}$ -AV-1451 uptake in patients with Alzheimer's disease and contrast these patterns with those that were expected in patients with PSP on the basis of previous studies (Johnson *et al.*, 2016; Ossenkoppele *et al.*, 2016; Schöll *et al.*, 2016; Schwarz *et al.*, 2016).

The value of comparing these two clinical groups lies not in their differential diagnosis, which is clear on clinical grounds alone, but in testing the ligand's binding against well-established clinico-pathological correlations and distinct distributions of tau pathology. These two disorders represent different kinds of tauopathy, with paired helical versus straight filamentous tau. Evidence on  $^{18}\text{F}$ -AV-1451's binding distributions, its off-target binding, and clinical correlations would directly inform the design of forthcoming clinical trials of anti-tau therapies in these diseases.

Overall, we aimed to: (i) identify the patterns of  $^{18}\text{F}$ -AV-1451 binding in patients with Alzheimer's disease, relative to patients with PSP as well as sex- and age-matched healthy controls; (ii) test whether  $^{18}\text{F}$ -AV-1451 binding was associated with disease severity in Alzheimer's disease and PSP; and (iii) assess whether regional  $^{18}\text{F}$ -AV-1451 binding could distinguish between Alzheimer's disease and PSP groups. We combined patients with clinical diagnostic criteria for Alzheimer's disease and MCI patients who had biomarker evidence of Alzheimer's disease pathology (i.e. with a positive scan for amyloid), based on the fact that these two groups represent a continuum of disease (Okello *et al.*, 2009). In view of the suggested effect of off-target binding, we also examined  $^{18}\text{F}$ -AV-1451 uptake in relation to AT8 immunohistochemistry of hyperphosphorylated tau protein and tinctorial stain for neuromelanin, in post-mortem sections from a patient with Alzheimer's disease, PSP, and a similarly aged control from the Cambridge Brain Bank.

Our principal hypotheses were that: (i) patients with Alzheimer's disease and those with MCI and PET scans positive for amyloid would show increased  $^{18}\text{F}$ -AV-1451 binding in the cortical and subcortical areas associated with

Alzheimer's pathology, including the medial temporal lobe as well as frontal, parietal, and temporal cortices (Serrano-Pozo *et al.*, 2011); (ii) patients with PSP would display increased  $^{18}\text{F}$ -AV-1451 binding especially in the midbrain and basal ganglia, with likely additional binding in frontal cortex (including the motor areas) and supramarginal gyrus, a set of subcortical and cortical regions that have been shown to display tau pathology in PSP (Schofield *et al.*, 2005; Dickson *et al.*, 2007; Smith *et al.*, 2016); and (iii) PSP and Alzheimer's disease patients would be distinguishable based on the regional  $^{18}\text{F}$ -AV-1451 binding levels, particularly in the hippocampus and midbrain, two key subcortical regions that show highly distinct neuropathological changes in Alzheimer's disease and PSP, respectively.

## Materials and methods

### Participants

The current study was conducted within the context of the Neuroimaging of Inflammation in Memory and Other Disorders (NIMROD) project (Bevan-Jones *et al.*, 2016a). We recruited 19 patients with PSP [*'probable PSP'* by Movement Disorder Society criteria (Litvan *et al.*, 1996a, b), representing the *'classical phenotype'*, which is sometimes referred to as Richardson's syndrome], nine patients meeting diagnostic criteria for probable Alzheimer's disease (McKhann *et al.*, 2011), and six patients with MCI and biomarker evidence of Alzheimer's disease (i.e. amyloid pathology). MCI was defined as a Mini-Mental Score Examination (MMSE) >24 with a memory impairment at least 1.5 standard deviations (SD) below that expected for age and education (Petersen *et al.*, 1999). All participants with MCI had a positive Pittsburgh compound B (PiB) PET scan (assessing *in vivo* amyloid pathology). Thirteen age- and sex-matched healthy controls with no history of major psychiatric or neurological illnesses, head injury or any other significant medical co-morbidity were also included to allow group-wise comparisons with the clinical cohorts. All participants were aged over 50 years, had sufficient proficiency in English for cognitive testing and had no contraindications to MRI. Patients and healthy controls were identified from the specialist clinics for memory disorders and PSP at the Cambridge University Hospitals NHS Trust and from registers held by the Dementias and Neurodegenerative Diseases Research Network (DeNDRoN); part of the NIHR Clinical Research Network. All participants had full mental capacity and provided written informed consent which was approved by the local ethical committee, in accord to the Declaration of Helsinki. As some of the assessment scales required carers' input for completion, we also obtained informed written consent from contributory carers.

### Clinical and neuroimaging assessment

#### Clinical and cognitive assessment

Participants underwent an initial assessment that included clinical indices of disease severity (e.g. Progressive Supranuclear Palsy Rating Scale) (Golbe and Ohman-Strickland, 2007),

demographic measures, and neuropsychological tests [MMSE and Addenbrooke's Cognitive Examination-Revised (ACE-R)].

### MRI data acquisition and preprocessing

Participants underwent an MRI session acquired on a 3 T scanner (Siemens Magnetom Tim Trio and Verio scanner; www.medical.siemens.com) using a MP-RAGE T<sub>1</sub>-weighted sequence (all groups). The T<sub>1</sub>-weighted sequence (repetition time = 2300 ms, echo time = 2.98 ms, field of view = 240 × 256 mm<sup>2</sup>, 176 slices of 1 mm thickness, flip angle = 9°) was used to facilitate tissue class segmentation (grey and white matter, together with CSF), and to allow non-rigid registration of standard space regions of interest (using a modified version of the Hammers atlas that included the midbrain and dentate nucleus of the cerebellum) (Hammers *et al.*, 2003) to subject MRI space. Each T<sub>1</sub> image was non-rigidly registered to the ICBM2009a template brain using ANTS (<http://www.picsl.upenn.edu/ANTS/>) and the inverse transform was applied to the Hammers atlas (resliced from MNI152 to ICBM2009a space) to bring the regions of interest to subject MRI space.

### PET data acquisition and preprocessing

All participants (i.e. patients with Alzheimer's disease, with MCI, with PSP, and control subjects) underwent <sup>18</sup>F-AV-1451 PET imaging to assess the extent and intensity of brain tau pathology. Subjects with MCI also underwent <sup>11</sup>C-PiB PET imaging to assess the density of amyloid-β deposits as an indication of Alzheimer's disease amyloid pathology. All radioligands were prepared at the Wolfson Brain Imaging Centre (WBIC), University of Cambridge, with high radiochemical purity (>95%). <sup>11</sup>C-PiB was produced with specific activity of >150 GBq/μmol, while <sup>18</sup>F-AV-1451 specific activity was of 216 ± 60 GBq/μmol at the end of synthesis. PET scanning was performed on a GE Advance PET scanner (GE Healthcare) and a GE Discovery 690 PET/CT. A 15-min <sup>68</sup>Ge/<sup>68</sup>Ga transmission scan was used for attenuation correction on the Advance, which was replaced by a low dose CT scan on the Discovery 690. The emission protocols were the same on both scanners: 550 MBq <sup>11</sup>C-PiB injection followed by imaging from 40–70 min post-injection and 90 min dynamic imaging (58 frames) following a 370 MBq <sup>18</sup>F-AV-1451 injection.

Each emission frame was reconstructed using the PROMIS 3D filtered back projection algorithm into a 128 × 128 matrix 30 cm transaxial field of view, with a transaxial Hann filter cut-off at the Nyquist frequency (Kinahan and Rogers, 1989). Corrections were applied for randoms, dead time, normalization, scatter, attenuation, and sensitivity. Each emission image series was aligned using SPM8 to correct for patient motion during data acquisition ([www.fil.ion.ucl.ac.uk/spm/software/spm8](http://www.fil.ion.ucl.ac.uk/spm/software/spm8)).

The mean aligned PET image, and hence the corresponding aligned dynamic PET image series, was rigidly registered to the T<sub>1</sub>-weighted image using SPM8 to extract values from both the Hammers atlas regions of interest and those in a reference tissue defined in the superior grey matter of the cerebellum using a 90% grey matter threshold on the grey matter probability map produced by SPM8 smoothed to PET resolution. The superior cerebellum was used as reference region as it is considered to have little or no tau pathology in either PSP or Alzheimer's disease (Williams *et al.*, 2007; Okello *et al.*, 2009;

Dickson, 2010; Schöll *et al.*, 2016; Schwarz *et al.*, 2016). This was confirmed in our post-mortem cases (Supplementary material). All region of interest data, including the reference tissue values, were corrected for CSF partial volumes through division with the mean region of interest probability (normalized to 1) of grey plus white matter segments, each smoothed to PET resolution. To test whether correction for CSF affected the main results, we repeated all the <sup>18</sup>F-AV-1451 PET analyses using data not corrected for CSF (see 'PET statistical analyses' and 'Results' sections).

<sup>11</sup>C-PiB data were quantified using SUVR by dividing the mean CSF-corrected radioactivity concentration in each region of interest by the corresponding mean radioactivity concentration in the reference tissue region of interest (whole cerebellum). For <sup>18</sup>F-AV-1451 non-displaceable binding potential (BP<sub>ND</sub>), a measure of specific binding, was determined for each Hammers atlas region of interest using a basis function implementation of the simplified reference tissue model (SRTM) operating upon the Hammers atlas and reference tissue region of interest data, both with and without CSF correction (Gunn *et al.*, 1997). <sup>11</sup>C-PiB data were treated as dichotomous measures (i.e. positive or negative) and considered positive if the ratio of the average SUVR values across the cortical and cerebellar regions of interest was >1.5, as previously described (Hatashita and Yamasaki, 2013).

### PET statistical analyses

To compare <sup>18</sup>F-AV-1451 binding across groups (Alzheimer's disease/MCI PiB+, PSP, and controls), individual region of interest BP<sub>ND</sub> values for <sup>18</sup>F-AV-1451 were used in a repeated-measures general linear model (GLM) to test for the main effect of region of interest, main effect of group, and group × region of interest interaction. Age and education were included as covariates of no interest. For the Alzheimer's disease/MCI PiB+ and PSP groups, we tested for correlations between regional <sup>18</sup>F-AV-1451 BP<sub>ND</sub> and disease severity using the ACE-R scores for Alzheimer's disease/MCI PiB+ patients and the Progressive Supranuclear Palsy Rating Scale for PSP patients with Pearson's correlation (with partial correlations accounting for age and education). All analyses were repeated using <sup>18</sup>F-AV-1451 BP<sub>ND</sub> values that were not corrected for CSF partial volume effects. To assess the ability of <sup>18</sup>F-AV-1451 BP<sub>ND</sub> to distinguish Alzheimer's disease patients from PSP cases, subject-specific <sup>18</sup>F-AV-1451 data in a set of regions of interest were input as key features in a support vector machine (SVM), a multivariate supervised statistical learning method suitable for neuroimaging modalities (Cortes and Vapnik, 1995). A reduced group of regions of interest considered as the most characteristic regions of interest affected by tau pathology in Alzheimer's disease and PSP was selected (i.e. superior/inferior temporal cortex, lateral occipital cortex, inferior parietal cortex, and hippocampus for Alzheimer's disease, and basal ganglia and midbrain for PSP); noting that the regions of interest included in the SVM were identical for both groups. This extended the whole-brain hierarchical cluster analysis described in the Supplementary material. The accuracy of each region of interest to discriminate between the Alzheimer's disease and PSP groups was computed using an SVM classifier with a K means cross-validation (K = 5) scheme with a linear kernel and standard cost parameter of 1.

## Neuropathological methods

### Tissue samples preparation

Post mortem brain tissue from three subjects (one Alzheimer's disease case, one PSP patient, and one healthy control with similar age) from the Cambridge Brain Bank was included in this study. The autoradiographic and immunohistochemical analyses were conducted in different cases from those included in the PET *in vivo* study. Tissue collection was approved by the local institutional review board. Neuropathological diagnoses were performed according to standardized protocols, on 15 blocked regions of cortex and subcortical regions. For this study, additional blocks of frozen brain tissue were obtained from the anterior hippocampus, midbrain, basal ganglia, and frontal cortex. Sections (20- $\mu$ m thick) were cut in a cryostat (Leica CM3050S S Research Cryostat) mounted on Thermo Scientific superfrost plus slides and used for  $^{18}\text{F}$ -AV-1451 phosphor screen, phosphorylated-tau immunoreactivity (AT8), and tinctorial stain for neuromelanin (Masson-Hamperl stain).

### $^{18}\text{F}$ -AV-1451 phosphor screen autoradiography

$^{18}\text{F}$ -AV-1451 for autoradiographic studies was synthesized in the same way as described above.  $^{18}\text{F}$ -AV-1451 phosphor screen autoradiography was performed following a previously published protocol by Marquìè and collaborators (2015). In brief, 20- $\mu$ m-thick frozen brain sections were fixed in 100% methanol at room temperature for 20 min and then transferred to a bath containing high specific activity  $^{18}\text{F}$ -AV-1451 in 10 mM phosphate-buffered saline (PBS) with a radioactivity concentration of  $\sim 20 \mu\text{Ci/ml}$ . Adjacent brain slices were placed in a bath that was identical in all aspects except that unlabelled AV-1451 was added to yield 1  $\mu\text{M}$  chemical concentration, a blocking condition sufficient to saturate essentially all available specific binding sites of tau. After incubation for 60 min, racks of slides were removed from the respective radioactive solutions and briefly incubated in a series of wash baths to remove unbound radiotracer. Wash solutions and incubation times were: 10 mM PBS for 1 min, 70% ethanol/30% PBS for 2 min, 30% ethanol/70% PBS for 1 min, and lastly 100% 10 mM PBS for 1 min. Racks were removed from the final wash solution, and slides were allowed to air dry before transfer to a storage phosphor screen (GE healthcare) that had been photobleached immediately before by exposure on a white light box for a minimum of 15 min. The slides and phosphor screen were enclosed in an aluminium film cassette and set away from sources of radioactivity for the

duration of the overnight exposure period. The cassette was opened and the slides were removed from the exposed screen, which was mounted on the digital imaging system (CR 35 BIO, Durr medical). Scanning of screens was controlled by Aida Image Analyser v.4.27 using 600 dpi resolution ( $\sim 42 \mu\text{m}$  sampling interval). Digital images were saved at full resolution and pixel depth. Images from adjacent brain slices incubated in the unblocked (high specific activity  $^{18}\text{F}$ -AV-1451 only) and blocking ( $^{18}\text{F}$ -AV-1451 plus 1  $\mu\text{M}$  unlabelled AV-1451) conditions were compared to estimate total and non-specific binding of  $^{18}\text{F}$ -AV-1451.

## Results

### Demographics and cognitive variables of patients in the PET *in vivo* study

There were no statistically significant differences between patient and control groups in terms of age or sex (Table 1). Shorter education was reported by patients with PSP relative to other groups (Table 1). One interpretation of this difference is that control cohorts over-represent people from higher socio-economic groups and with longer education; however, low education and its effects on health may also be a risk factor for the development of PSP (Litvan *et al.*, 2016). Age and education were included as covariates of no interest in the statistical models assessing the main effect of region, main effect of group, and group  $\times$  region of interest interactions. As expected, there was a significant main effect of group for cognitive measures, driven by reduced MMSE and ACE-R scores in Alzheimer's disease/MCI+ and PSP patients relative to healthy controls (Table 1).

### $^{18}\text{F}$ -AV-1451 binding in relation to clinical diagnosis

The mean  $^{18}\text{F}$ -AV-1451  $\text{BP}_{\text{ND}}$  PET map in each group (Fig. 1) and quantitative region of interest analyses (Fig. 2), indicated high  $^{18}\text{F}$ -AV-1451 binding in the basal ganglia in all groups including controls. In the repeated-measures ANOVA

**Table 1** Participant details and group differences by one-way ANOVA or chi-squared test

	AD/MCI+ (n = 15)	PSP (n = 19)	Healthy controls (n = 13)	Group difference
Sex (male/female)	9/6	11/8	6/7	N/S
Age, years (SD, range)	71.6 ( $\pm 8.7$ , 54–85)	69.5 ( $\pm 5.8$ , 52–79)	67.2 ( $\pm 7.3$ , 55–80)	$F = 1.2$ , $P = 0.3$
Education, years (SD, range)	14.3 ( $\pm 3.3$ , 10–19)	11.9 ( $\pm 1.8$ , 10–17)	15.8 ( $\pm 1.9$ , 11–19)	$F = 10.2$ , $P = 0.0003$
MMSE (SD, range)	25.5 ( $\pm 2.8$ , 18–28)	26.1 ( $\pm 4.5$ , 13–30)	29.3 ( $\pm 0.7$ , 28–30)	$F = 4.9$ , $P = 0.012$
ACE-R (SD, range)	75.9 ( $\pm 11.0$ , 51–89)	78.7 ( $\pm 15.8$ , 36–95)	95.5 ( $\pm 3.0$ , 89–99)	$F = 10.3$ , $P = 0.0002$
PSP Rating Scale (SD, range)	–	43.6 ( $\pm 15.8$ , 15–74)	–	–

Values are mean ( $\pm$ SD, range).

AD/MCI+ = Alzheimer's disease/mild cognitive impairment (amyloid-positive from PiB-PET scan); MMSE = Mini-Mental State Examination; ACE-R = Addenbrookes' Cognitive Examination, Revised. N/S = not significant at  $P < 0.05$  (uncorrected).

of regional binding, we found a significant main effect of group [ $F(2,41) = 17.5$ ,  $P = 0.00001$ ] and a region of interest  $\times$  group interaction [ $F(2,68) = 7.5$ ,  $P < 0.00001$ ], although there was no main effect of regions of interest [ $F(2,34) = 0.8$ ,  $P = 0.8$ ] (Fig. 2). The group and interaction effects were driven in part by greater  $^{18}\text{F}$ -AV-1451  $\text{BP}_{\text{ND}}$  in the Alzheimer's disease/MCI+ group relative to the PSP and control groups, in cortical and subcortical areas including frontal, parietal, lateral temporal, and occipital cortices as well as the hippocampus and other medial temporal lobe regions (*post hoc t*-tests,  $t$ 's  $> 2.2$ ,  $P$ 's  $< 0.04$ ) (Fig. 2). The PSP group, relative to the Alzheimer's disease group, showed increased  $^{18}\text{F}$ -AV-1451  $\text{BP}_{\text{ND}}$  in the midbrain ( $t = 2.1$ ,  $P < 0.04$ ); while, relative to controls, PSP patients showed increased  $^{18}\text{F}$ -AV-1451  $\text{BP}_{\text{ND}}$  in the putamen, pallidum, thalamus, midbrain, and dentate nucleus of the cerebellum ( $t$ 's  $> 2.7$ ,  $P < 0.02$ ) (Fig. 2).

Repeating the analyses using  $^{18}\text{F}$ -AV-1451  $\text{BP}_{\text{ND}}$  values that were not corrected for CSF partial volume effects yielded similar results [ $F(2,36) = 1.1$ ,  $P = 0.2$ , for the main effect of regions of interest;  $F(2,41) = 16.7$ ,  $P < 0.00001$  for the main effect of group; and  $F(2,72) = 6.3$ ,  $P < 0.00001$  for the group  $\times$  region of interest interaction]. We then tested whether regional  $^{18}\text{F}$ -AV-1451  $\text{BP}_{\text{ND}}$  related to disease severity. In the Alzheimer's disease/MCI+ group, there was no significant correlation between ACE-R score and  $^{18}\text{F}$ -AV-1451  $\text{BP}_{\text{ND}}$  in any region of interest ( $P$ 's  $> 0.14$ ). Similarly, in the PSP group, we found no significant correlation between  $^{18}\text{F}$ -AV-1451  $\text{BP}_{\text{ND}}$  in any region of interest and disease severity, as assessed via the Progressive

Supranuclear Palsy Rating Scale ( $P$ 's  $> 0.16$ ). Repeating the correlation analyses when using the  $^{18}\text{F}$ -AV-1451  $\text{BP}_{\text{ND}}$  values that were not corrected for CSF volume yielded similar non-significant results ( $P$ 's  $> 0.1$ ).

## Classification of cases by $^{18}\text{F}$ -AV-1451 $\text{BP}_{\text{ND}}$

The SVM analysis using  $^{18}\text{F}$ -AV-1451  $\text{BP}_{\text{ND}}$  values in a subset of regions of interest was able to separate the Alzheimer's disease/MCI+ patients from PSP cases with a classification accuracy of 94.1%. The accuracy for the other pair-wise comparisons is as follows: Alzheimer's disease/MCI+ versus controls = 85.7%; PSP versus controls = 90.6% (Fig. 3 for data plot from two characteristic regions of interest). In the Supplementary material we also report the accuracy of pair-wise comparisons between groups using hierarchical cluster analyses, based on the regional distribution of  $^{18}\text{F}$ -AV-1451  $\text{BP}_{\text{ND}}$  across the whole brain (Bevan Jones *et al.*, 2016a).

## Phosphor screen autoradiography and immunohistochemistry post-mortem

A summary of the autoradiography results, AT8 immunohistochemistry data, and neuromelanin staining in post-mortem Alzheimer's disease, PSP, and control case is shown in Fig. 4.

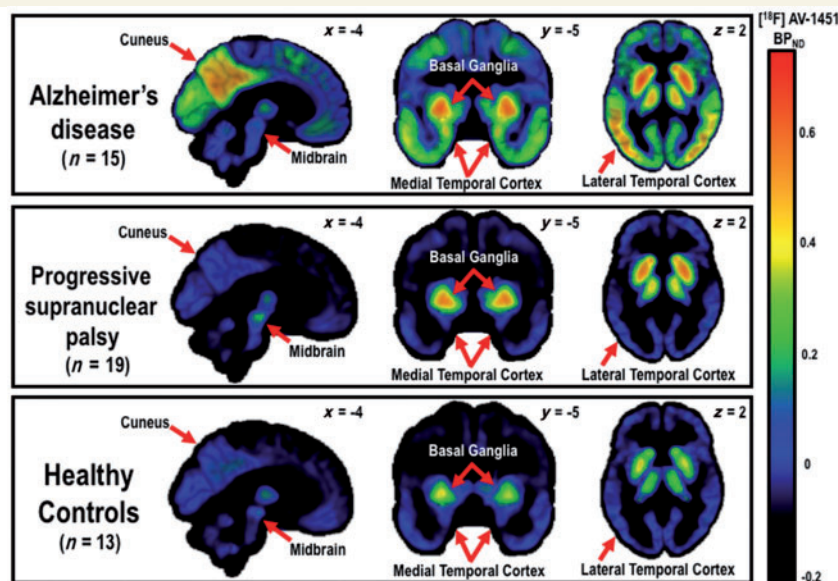


**Figure 1**  $\text{BP}_{\text{ND}}$  for  $^{18}\text{F}$ -AV-1451 for Alzheimer's disease, including PiB positive MCI, PSP, and healthy controls. Note the  $^{18}\text{F}$ -AV-1451 binding in the basal ganglia in all groups, albeit higher in Alzheimer's disease and PSP patients. Patients with Alzheimer's disease also showed increased  $^{18}\text{F}$ -AV-1451 binding in medial temporal lobe regions and widespread neocortical areas, relative to controls and PSP patients, while PSP patients had increased high  $^{18}\text{F}$ -AV-1451 binding to the midbrain, relative to patients with Alzheimer's disease and control subjects (see Fig. 2 and 'Results' section in the main text for quantitative analyses).

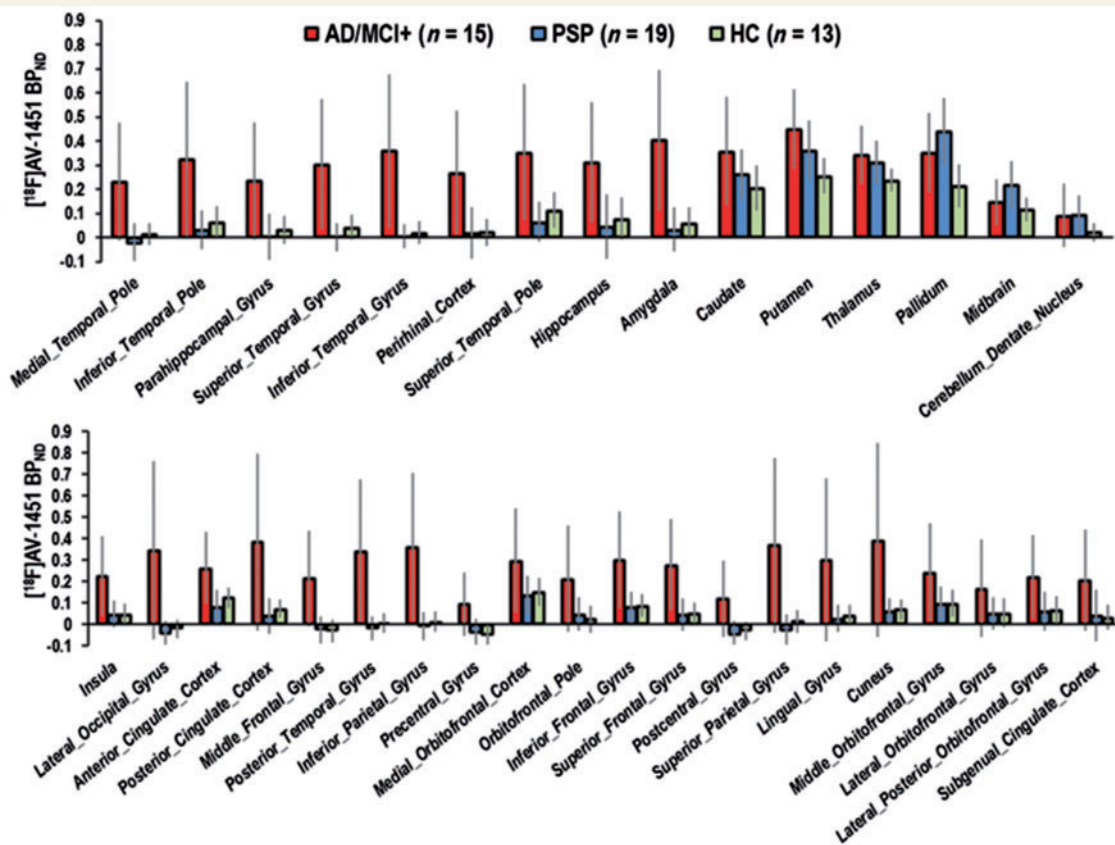


**Figure 2** Mean ( $\pm$ SD)  $^{18}\text{F}$ -AV-1451  $\text{BP}_{\text{ND}}$  in each region of interest for the participant groups: Alzheimer’s disease and amyloid-positive MCI; PSP, and healthy controls. The  $^{18}\text{F}$ -AV-1451  $\text{BP}_{\text{ND}}$  data reported here are corrected for CSF volume. See the ‘Results’ section for statistics related to CSF corrected and uncorrected data. AD = Alzheimer’s disease; MCI+ = amyloid-positive MCI; HC = healthy control.

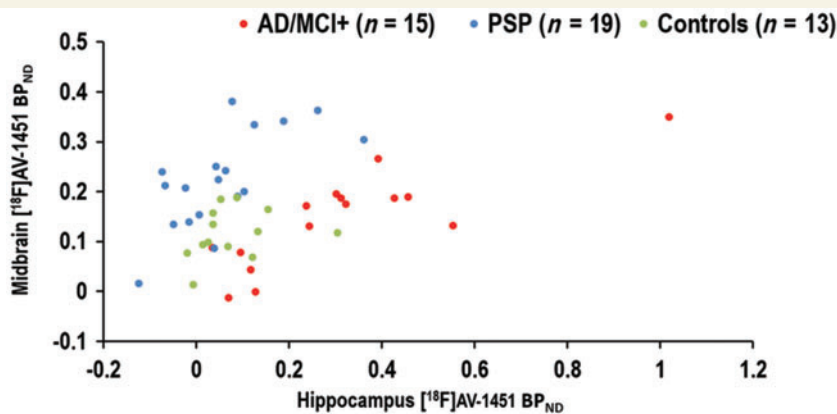


**Figure 3** Individual  $^{18}\text{F}$ -AV-1451  $\text{BP}_{\text{ND}}$  values in the hippocampus (x-axis) and midbrain (y-axis) in patients with Alzheimer’s disease (AD) and amyloid-positive MCI (MCI+; red dots), PSP (cyan dots), and healthy control subjects (green dots). Note the clear bivariate separation of AD/MCI+ from PSP patients.

The autoradiography phosphor screen analyses in the Alzheimer’s disease brain tissue sample revealed that the hippocampus had the highest and most specific binding of the  $^{18}\text{F}$ -AV-1451 radiotracer.  $^{18}\text{F}$ -AV-1451 binding was also found in the frontal cortex in the Alzheimer’s disease case, although to a lesser extent than in the hippocampal

slice. In contrast, sparse and non-specific  $^{18}\text{F}$ -AV-1451 binding was found in the Alzheimer’s disease basal ganglia tissue.

The PSP and control tissues showed overall sparse and non-specific  $^{18}\text{F}$ -AV-1451 binding, including hippocampus, midbrain, basal ganglia, and frontal cortex.

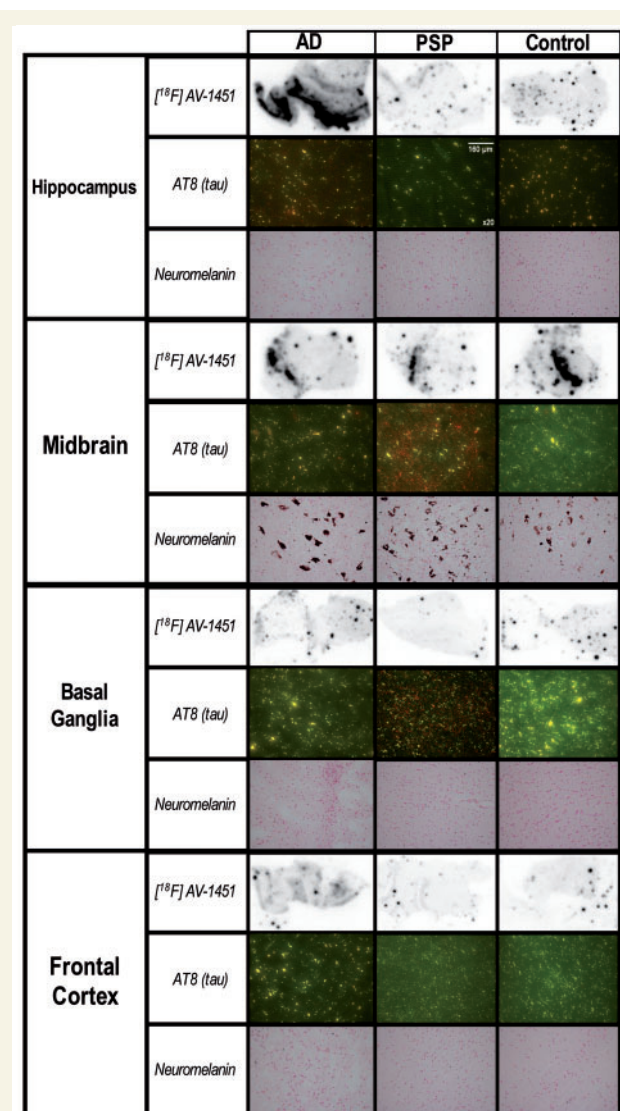


**Figure 4 Post-mortem data.** The figure aligns the  $^{18}\text{F}$ -AV-1451 autoradiographic binding in key regions of interest in an Alzheimer's disease (AD) case, a patient with PSP, and a control of similar age. Immunohistochemistry data assessing hyperphosphorylated tau (AT8, red), and neuromelanin staining (dark brown) are also shown for the same cases and regions of interest. There is  $^{18}\text{F}$ -AV-1451 binding in the hippocampus and, to a lesser extent, in the frontal cortex in Alzheimer's disease. In contrast,  $^{18}\text{F}$ -AV-1451 binding to the midbrain slices was not specific to PSP but was also detected in the Alzheimer's disease and control cases, who showed little or no tau pathology in the midbrain. Despite the *in vivo*  $^{18}\text{F}$ -AV-1451 binding to the basal ganglia in all groups (including controls, see Figs 1 and 2), post-mortem  $^{18}\text{F}$ -AV-1451 binding to the basal ganglia was sparse and non-specific in these three cases. Note the absence of neuromelanin-containing cells in the basal ganglia and cortical regions. The magnification of the immunohistochemistry pictures (AT8) and neuromelanin staining is  $\times 20$ .

Abundant hyperphosphorylated tau protein was detected in the hippocampus of the Alzheimer's disease case, while small and punctate tau staining was found in the midbrain

and frontal cortex of the same patient, which is overall consistent with the results of the phosphor screen autoradiography. Although hyperphosphorylated tau protein was found in the frontal cortex in the Alzheimer's disease case, its relatively low density could be due to a slow cortical disease progression in this particular patient.

The PSP tissue displayed high concentration of hyperphosphorylated tau in the midbrain and basal ganglia, while the Alzheimer's disease brain displayed little AT8 staining in the basal ganglia.

As expected, the control brain did not show AT8 immunoreactivity in any of the regions of interest examined.

Neuromelanin-containing cells were only observed in the midbrain in all post-mortem cases. Of note, no neuromelanin-containing cells were found in the basal ganglia in either the Alzheimer's disease, PSP or control case, which is in contrast to the strong *in vivo*  $^{18}\text{F}$ -AV-1451 binding of this radiotracer to the same region of interest.

## Discussion

The principal result of our study is that PET imaging with the radiotracer  $^{18}\text{F}$ -AV-1451 revealed distinct patterns of binding in Alzheimer's disease and its prodromal state of MCI, in comparison to the primary tauopathy of PSP. The relatively large size of our PET study confirmed the high accuracy of discrimination between the clinical groups using  $^{18}\text{F}$ -AV-1451  $\text{BP}_{\text{ND}}$  data, with a simple support vector machine and indeed by visual inspection (Figs 1, 2 and 3). However, despite this heuristic potential of  $^{18}\text{F}$ -AV-1451 as a tau biomarker, caution in the interpretation of its binding targets is indicated by the neuropathological and autoradiographic data (Marquì *et al.*, 2015). In particular, while  $^{18}\text{F}$ -AV-1451 strongly bound to Alzheimer's disease-related tau pathology, non-specific binding of the same tracer can be found in patients with PSP and control subjects (Marquì *et al.*, 2015). Nevertheless, our post-mortem data suggest that off-target binding to neuromelanin is not a sufficient explanation of the  $\text{BP}_{\text{ND}}$  for  $^{18}\text{F}$ -AV-1451, at least in the context of PSP, and in some critical regions as the basal ganglia. For instance, we found *in vivo* significant  $^{18}\text{F}$ -AV-1451 binding in the basal ganglia (in all groups including controls) in the absence of post-mortem neuromelanin-containing cells. This indicates that neuromelanin is not the principal target of off-target binding for  $^{18}\text{F}$ -AV-1451, but there may be other off-target binding sites that have as yet not been identified, including non-tau targets in disorders associated with predominantly TDP-43 pathology (Bevan-Jones *et al.*, 2016c).

For  $^{18}\text{F}$ -AV-1451 PET to meet its full potential as a biomarker to stratify or monitor the effect of disease-modifying drugs in future clinical trials, additional properties would therefore need to be established. In particular, further work is needed to demonstrate changes in  $^{18}\text{F}$ -AV-1451 PET over time, or in response to treatment. A cross-sectional study as this one cannot be used to infer

longitudinal changes, but it can be employed to inform and model a biomarker's potential. More specifically, the relevance of  $^{18}\text{F}$ -AV-1451 is increased by the demonstration that its binding patterns recapitulate *in vivo* the established post-mortem distributions of tau pathology in Alzheimer's disease and PSP. In addition,  $^{18}\text{F}$ -AV-1451 PET may have biomarker potential for the differential diagnosis of equivocal cases: while the distinction between Alzheimer's disease and PSP can be readily made on clinical grounds, patients with PSP-parkinsonism clinically resemble Parkinson's disease (Williams *et al.*, 2005).

In contrast to previous results (Johnson *et al.*, 2016; Ossenkoppele *et al.*, 2016),  $^{18}\text{F}$ -AV-1451 binding was not correlated with disease severity in our groups (i.e. severity of cognitive impairment in patients with Alzheimer's disease and Progressive Supranuclear Palsy Rating Scale in patients with PSP). There are several possible explanations for the lack of a correlation in our study, including lack of statistical power (type II error) or the use of clinical measures that were not sufficiently sensitive to describe the full spectrum of clinical variability in Alzheimer's disease and PSP. Alternatively, it may be that  $^{18}\text{F}$ -AV-1451 binding is inherently limited in staging disease severity in Alzheimer's disease and PSP, analogous to the PiB tracer in Alzheimer's disease (Hatashita and Yamasaki, 2010).

Technical considerations in assessing the  $^{18}\text{F}$ -AV-1451 binding post-mortem and in estimating  $\text{BP}_{\text{ND}}$  *in vivo* must also be discussed. First, it is possible that in the autoradiographic protocol (Marquié *et al.*, 2015), ethanol washing, and other procedures may have affected the labelling with  $^{18}\text{F}$ -AV-1451, especially in the basal ganglia. Second, our PET analyses employed correction of 'partial volume effects', resulting from CSF volume within each region. This mitigates the potential influence of brain volume loss seen in Alzheimer's disease and PSP. Nevertheless, using uncorrected PET data yielded qualitatively similar results in terms of the main effect of group and group  $\times$  region of interest interaction, which suggests that we avoided 'over-correcting' the  $\text{BP}_{\text{ND}}$  values based on cortical and subcortical atrophy, and the consequent inferential error from CSF volume and its correction.

Interestingly, the regions with the most significant group differences in  $^{18}\text{F}$ -AV-1451  $\text{BP}_{\text{ND}}$  in Alzheimer's disease and PSP *in vivo* were those predicted from prior post-mortem studies for each disease. More specifically, the clinical syndromes of Alzheimer's disease and biomarker positive MCI were associated with increased  $^{18}\text{F}$ -AV-1451  $\text{BP}_{\text{ND}}$  in widely distributed sub-cortical and cortical areas that have been consistently implicated in the pathogenesis and progression of Alzheimer's disease (e.g. hippocampus, amygdala as well as frontal, parietal, temporal, and occipital cortices) (Braak and Braak, 1995). Conversely, PSP was associated with a pattern of increased  $^{18}\text{F}$ -AV-1451  $\text{BP}_{\text{ND}}$  in the basal ganglia, midbrain, and dentate nucleus of the cerebellum, consistent with the pathophysiology of the disease (Hauw *et al.*, 1994; Litvan *et al.*, 1996a, b). Together, these data demonstrated that the  $^{18}\text{F}$ -AV-1451 ligand

recapitulates *in vivo* the typical neuropathological changes seen in Alzheimer's disease and PSP, although it cannot be assumed that the cellular and/or molecular targets of  $^{18}\text{F}$ -AV-1451 binding are the same in both disorders.

$^{18}\text{F}$ -AV-1451  $\text{BP}_{\text{ND}}$  in selected regions of interest also distinguished Alzheimer's disease cases from PSP patients with an accuracy of 94% which suggests the potential of this radio-tracer to discriminate *in vivo* among different tauopathies. The value of this analysis is obviously not as a diagnostic biomarker, as clinical features readily distinguish the groups, but rather represents an early step in the process of validating  $^{18}\text{F}$ -AV-1451 PET as a biomarker for tauopathies. Multicentre replication with larger samples and broader diagnostic spectra are necessary, including for example, patients with frontotemporal dementia, corticobasal syndrome, or presymptomatic individuals with high risk of developing tau-related neurodegenerative disorders (e.g. carrying specific gene mutations).

Finally, we note that our data are specific to  $^{18}\text{F}$ -AV-1451, and do not necessarily generalize to other radioligands. Further work is required to determine the specificity of  $^{18}\text{F}$ -AV-1451 and other candidate ligands' binding to the different isoforms of tau protein, their differential modes of modification (e.g. phosphorylation, acetylation) and aggregation (e.g. oligomeric states or neurofibrillar tangles). These issues are of high relevance for this and other studies because: (i) Alzheimer's disease is characterized by balanced 3R/4R isoforms, while PSP pathology is mainly a 4R isoform tauopathy (Buée and Delacourte, 1999; Espinoza *et al.*, 2008); and (ii) the toxicity of tau aggregates may be driven by oligomers rather than tangles.

In conclusion, we suggest that  $^{18}\text{F}$ -AV-1451 is a useful PET ligand for *in vivo* studies in clinical populations with Alzheimer's disease pathology and non-Alzheimer's disease primary tauopathies such as PSP, despite the potential contribution of non-specific or 'off-target' binding. The brain regions with increased  $^{18}\text{F}$ -AV-1451 binding were those predicted from the well-established patterns of neurodegeneration in both diseases, and are in keeping with the cognitive and motor features classically seen in Alzheimer's disease and PSP clinical syndromes, respectively. Together, our current findings support the further use of  $^{18}\text{F}$ -AV-1451 PET *in vivo* and *in vitro* to evaluate tau pathology in studies of dementia and neurodegeneration.

## Acknowledgements

Thanks to our volunteers for participating in this study and to the radiographers/technologists at the Wolfson Brain Imaging Centre and PET/CT Unit, Addenbrooke's Hospital, for their invaluable support in data acquisition. We thank the NIHR Dementias and Neurodegenerative Diseases Research Network for help with subject recruitment. We thank Cambridge Brain Bank, part of the Cambridge Human Research Tissue Bank. We also thank Oliver Green for his technical assistance and Dr's Istvan

Boros, Joong-Hyun Chun, and WBIC RPU for the manufacture of  $^{18}\text{F}$ -AV-1451. We thank Avid (Lilly) for supplying the precursor for the manufacturing of AV-1451 for use in this study.

## Funding

This study was funded by the National Institute for Health Research (NIHR, RG64473) Cambridge Biomedical Research Centre and Biomedical Research Unit in Dementia, PSP Association, the Wellcome Trust (JBR 103838), the Medical Research Council of Cognition and Brain Sciences Unit, Cambridge (MC-A060-5PQ30), and partially by a Medical Research Council grant (MR/K02308X/1) held by J.T.O., J.B.R., and F.I.A. The Human Research Tissue Bank is supported by the NIHR Cambridge Biomedical Research Centre. None of the authors have conflicts of interest to report.

## Supplementary material

Supplementary material is available at *Brain* online.

## References

- Alexander SK, Rittman T, Xuereb JH, Bak TH, Hodges JR, Rowe JB. Validation of the new consensus criteria for the diagnosis of corticobasal degeneration. *J Neurol Neurosurg Psychiatry* 2014; 85: 925–9.
- Anderson JM, Hampton DW, Patani R, Pryce G, Crowther RA, Reynolds R, et al. Abnormally phosphorylated tau is associated with neuronal and axonal loss in experimental autoimmune encephalomyelitis and multiple sclerosis. *Brain* 2008; 131: 1736–48.
- Ballatore C, Lee VM-Y, Trojanowski JQ. Tau-mediated neurodegeneration in Alzheimer's disease and related disorders. *Nat Rev Neurosci* 2007; 8: 663–72.
- Bevan-Jones RW, Surendranathan A, Passamonti L, Vázquez-Rodríguez P, Arnold R, Mak E, et al. Neuroimaging of inflammation in memory and related other disorders (NIMROD) study protocol: a deep phenotyping cohort study of the role of brain inflammation in dementia, depression and other neurological illnesses. *BMJ Open* 2016a, in press. doi: 10.1136/bmjopen-2016-013187.
- Bevan-Jones WR, Cope TE, Passamonti L, Fryer TD, Hong YT, Aigbirhio F, et al. [ $^{18}\text{F}$ ]AV-1451 PET in behavioral variant frontotemporal dementia due to MAPT mutation. *Ann Clin Transl Neurol* 2016; 3: 940–7.
- Bevan-Jones WR, Cope TE, Passamonti L, Vázquez Rodríguez P, Surendranathan A, Arnold R, et al.  $^{18}\text{F}$ -AV1451 PET imaging in semantic dementia. *J Neurochem* 2016c; 138: 401.
- Bloom GS. Amyloid- $\beta$  and tau: the trigger and bullet in Alzheimer disease pathogenesis. *JAMA Neurol* 2014; 71: 505–8.
- Braak H, Braak E. Staging of alzheimer's disease-related neurofibrillary changes. *Neurobiol Aging* 1995; 16: 271–278.
- Braak H, Alafuzoff I, Arzberger T, Kretschmar H, Del Tredici K. Staging of Alzheimer disease-associated neurofibrillary pathology using paraffin sections and immunocytochemistry. *Acta Neuropathol* 2006; 112: 389–404.
- Buée L, Delacourte A. Comparative biochemistry of tau in progressive supranuclear palsy, corticobasal degeneration, FTDP-17 and Pick's disease. *Brain Pathol* 1999; 9: 681–93.
- Chien DT, Bahri S, Szardenings AK, Walsh JC, Mu F, Su M-Y, et al. Early clinical PET imaging results with the novel PHF-tau radioligand [ $^{18}\text{F}$ ]-T807. *J. Alzheimers Dis* 2013; 34: 457–68.
- Clavaguera F, Akatsu H, Fraser G, Crowther RA, Frank S, Hench J, et al. Brain homogenates from human tauopathies induce tau inclusions in mouse brain. *Proc Natl Acad Sci USA* 2013; 110: 9535–40.
- Cortes C, Vapnik V. Support-vector networks. *Mach Learn* 1995; 20: 273–97.
- de Calignon A, Polydoro M, Suárez-Calvet M, William C, Adamowicz DH, Kopeikina KJ, et al. Propagation of Tau pathology in a model of early Alzheimer's disease. *Neuron* 2012; 73: 685–97.
- Dickson DW, Rademakers R, Hutton ML. progressive supranuclear palsy: pathology and genetics. *Brain Pathol* 2007; 17: 74–82.
- Dickson DW, Ahmed Z, Algom AA, Tsuboi Y, Josephs KA. Neuropathology of variants of progressive supranuclear palsy. *Curr Opin Neurol* 2010; 23: 394–400.
- Espinoza M, de Silva R, Dickson DW, Davies P. Differential Incorporation of Tau Isoforms in Alzheimer's disease. *J Alzheimers Dis* 2008; 14: 1–16.
- Fernández-Nogales M, Cabrera JR, Santos-Galindo M, Hoozemans JJM, Ferrer I, Rozemuller AJM, et al. Huntington's disease is a four-repeat tauopathy with tau nuclear rods. *Nat Med* 2014; 20: 881–5.
- Goedert M, Wischik CM, Crowther RA, Walker JE, Klug A. Cloning and sequencing of the cDNA encoding a core protein of the paired helical filament of Alzheimer disease: identification as the microtubule-associated protein tau. *Proc Natl Acad Sci USA* 1988; 85: 4051–5.
- Golbe LI, Ohman-Strickland PA. A clinical rating scale for progressive supranuclear palsy. *Brain* 2007; 130: 1552–65.
- Gunn RN, Lammertsma AA, Hume SP, Cunningham VJ. Parametric imaging of ligand-receptor binding in PET using a simplified reference region model. *Neuroimage* 1997; 6: 279–87.
- Hammers A, Allom R, Koepp MJ, Free SL, Myers R, Lemieux L, et al. Three-dimensional maximum probability atlas of the human brain, with particular reference to the temporal lobe. *Hum Brain Mapp* 2003; 19: 224–47.
- Hansen AK, Knudsen K, Lillethorup TP, Landau AM, Parbo P, Fedorova T, et al. *In vivo* imaging of neuromelanin in Parkinson's disease using  $^{18}\text{F}$ -AV-1451 PET. *Brain* 2016; 139: 2039–49.
- Hatashita S, Yamasaki H. Clinically different stages of Alzheimer's disease associated by amyloid deposition with [ $^{11}\text{C}$ ]-PIB PET imaging. *J. Alzheimers Dis* 2010; 21: 995–1003.
- Hatashita S, Yamasaki H. Diagnosed mild cognitive impairment due to Alzheimer's disease with PET biomarkers of beta amyloid and neuronal dysfunction. *PLoS One* 2013; 8: e66877.
- Hauw JJ, Daniel SE, Dickson D, Horoupian DS, Jellinger K, Lantos PL, et al. Preliminary NINDS neuropathologic criteria for Steele-Richardson-Olszewski syndrome (progressive supranuclear palsy). *Neurology* 1994; 44: 2015–19.
- Hodges JR, Davies RR, Xuereb JH, Casey B, Broe M, Bak TH, et al. Clinicopathological correlates in frontotemporal dementia. *Ann Neurol* 2004; 56: 399–406.
- Irwin DJ, Lee VM-Y, Trojanowski JQ. Parkinson's disease dementia: convergence of  $\alpha$ -synuclein, tau and amyloid- $\beta$  pathologies. *Nat Rev Neurosci* 2013; 14: 626–36.
- Johnson KA, Schultz A, Betensky RA, Becker JA, Sepulcre J, Rentz D, et al. Tau PET imaging in aging and early Alzheimer's disease. *Ann Neurol* 2016; 79: 110–19.
- Kinahan PE, Rogers JG. Analytic 3D image reconstruction using all detected events. *IEEE Trans Nucl Sci* 1989; 36: 964–8.
- Litvan I, Agid Y, Calne D, Campbell G, Dubois B, Duvoisin RC, et al. Clinical research criteria for the diagnosis of progressive supranuclear palsy (Steele-Richardson-Olszewski syndrome): report of the NINDS-SPPS international workshop. *Neurology* 1996a; 47: 1–9.

- Litvan I, Hauw JJ, Bartko JJ, Lantos PL, Daniel SE, Horoupian DS, et al. Validity and reliability of the preliminary NINDS neuropathologic criteria for progressive supranuclear palsy and related disorders. *J Neuropathol Exp Neurol* 1996b; 55: 97–105.
- Litvan I, Lees PSJ, Cunningham CR, Rai SN, Cambon AC, Standaert DG, et al. Environmental and occupational risk factors for progressive supranuclear palsy: case-control study. *Mov Disord* 2016; 31: 644–52.
- Marquié M, Normandin MD, Vanderburg CR, Costantino IM, Bien EA, Rycyna LG, et al. Validating novel tau positron emission tomography tracer [F-18]-AV-1451 (T807) on postmortem brain tissue. *Ann Neurol* 2015; 78: 787–800.
- Maruyama M, Shimada H, Suhara T, Shinotoh H, Ji B, Maeda J, et al. Imaging of Tau pathology in a tauopathy mouse model and in Alzheimer patients compared to normal controls. *Neuron* 2013; 79: 1094–108.
- McKhann GM, Knopman DS, Chertkow H, Hyman BT, Jack CR, Kawas CH, et al. The diagnosis of dementia due to Alzheimer's disease: recommendations from the National Institute on Aging-Alzheimer's Association workgroups on diagnostic guidelines for Alzheimer's disease. *Alzheimers Dement* 2011; 7: 263–9.
- Murray ME, Kouri N, Lin W-L, Jack CR, Dickson DW, Vemuri P. Clinicopathologic assessment and imaging of tauopathies in neurodegenerative dementias. *Alzheimers Res Ther* 2014; 6: 1.
- Okamura N, Furumoto S, Fodero-Tavoletti MT, Mulligan RS, Harada R, Yates P, et al. Non-invasive assessment of Alzheimer's disease neurofibrillary pathology using 18F-THK5105 PET. *Brain* 2014; 137: 1762–71.
- Okello A, Koivunen J, Edison P, Archer HA, Turkheimer FE, Någren K, et al. Conversion of amyloid positive and negative MCI to AD over 3 years. *Neurology* 2009; 73: 754–60.
- Ossenkoppele R, Schonhaut DR, Baker SL, O'Neil JP, Janabi M, Ghosh PM, et al. Tau, Amyloid, and Hypometabolism in a Patient with Posterior Cortical Atrophy. *Ann Neurol* 2015; 77: 338–42.
- Ossenkoppele R, Schonhaut DR, Schöll M, Lockhart SN, Ayakta N, Baker SL, et al. Tau PET patterns mirror clinical and neuroanatomical variability in Alzheimer's disease. *Brain* 2016; 139: 1551–67.
- Petersen RC, Smith GE, Waring SC, Ivnik RJ, Tangalos EG, Kokmen E. Mild cognitive impairment: clinical characterization and outcome. *Arch Neurol* 1999; 56: 303–8.
- Schofield EC, Caine D, Kril JJ, Cordato NJ, Halliday GM. Staging disease severity in movement disorder tauopathies: brain atrophy separates progressive supranuclear palsy from corticobasal degeneration. *Mov Disord* 2005; 20: 34–9.
- Schöll M, Lockhart SN, Schonhaut DR, O'Neil JP, Janabi M, Ossenkoppele R, et al. PET imaging of tau deposition in the aging human brain. *Neuron* 2016; 89: 971–82.
- Schwarz AJ, Yu P, Miller BB, Shcherbinin S, Dickson J, Navitsky M, et al. Regional profiles of the candidate tau PET ligand 18F-AV-1451 recapitulate key features of Braak histopathological stages. *Brain* 2016; 139: 1539–50.
- Serrano-Pozo A, Frosch MP, Masliah E, Hyman BT. Neuropathological alterations in Alzheimer disease. *Cold Spring Harb Perspect Med* 2011; 1: a006189.
- Smith R, Schain M, Nilsson C, Strandberg O, Olsson T, Hägerström D, et al. Increased basal ganglia binding of (18) F-AV-1451 in patients with progressive supranuclear palsy. *Mov Disord* 2016, in press.
- Spillantini M, Goedert M. Tau and parkinson disease. *JAMA* 2001; 286: 2324–6.
- Williams DR, de Silva R, Paviour DC, Pittman A, Watt HC, Kilford L, et al. Characteristics of two distinct clinical phenotypes in pathologically proven progressive supranuclear palsy: Richardson's syndrome and PSP-parkinsonism. *Brain* 2005; 128: 1247–58.
- Williams DR, Holton JL, Strand C, Pittman A, de Silva R, Lees AJ, et al. Pathological tau burden and distribution distinguishes progressive supranuclear palsy-parkinsonism from Richardson's syndrome. *Brain* 2007; 130: 1566–76.
- Xia C-F, Arteaga J, Chen G, Gangadharmath U, Gomez LF, Kasi D, et al. [(18)F]T807, a novel tau positron emission tomography imaging agent for Alzheimer's disease. *Alzheimers Dement* 2013; 9: 666–76.